spectively. Using the measured range of 0–2 kcal/mol for the activation energy for ammonia decomposition on Pt(110)-(1 × 2) yields a reaction probability of (1–2.8) × 10^{-3} at $1/T = 0$. The measured reaction probability at $1/T = 0$ for the polycrystalline platinum surface is (2.4–3.3) × 10^{-3}.[3] On the basis of the model embodied by eq 1–4, the rate of ammonia decomposition in this regime is controlled by a competition between the rate of cleavage of an N–H bond and the rate of desorption of molecularly adsorbed ammonia. The observed activation energy is therefore given by $E_r - E_{d,NH_3}$.[3] Values for E_r and/or E_{d,NH_3}, individually accurate to within the measured difference in activation energy of approximately 3 kcal/mol, are not available. Thus a determination of the relative contributions from changes in E_r and/or E_{d,NH_3} is precluded. The observed difference in activation energies and the similarity of the reaction probabilities at $1/T = 0$ indicate, however, that for finite temperatures ($1/T > 0$) where the rate of decomposition is linearly dependent on ammonia pressure the reaction probability on the Pt(110)-(1 × 2) surface is greater than that on the polycrystalline surface. For example, at 2 × 10^{-6} Torr and 800 K, the reaction probabilities are 1.6 × 10^{-3} and 2.0 × 10^{-4} on the Pt(110)-(1 × 2) and the polycrystalline platinum surfaces, respectively.

5. Synopsis

The results of this study may be summarized as follows:

1. The steady-state decomposition kinetics of ammonia on Pt(110)-(1 × 2) are qualitatively similar to those observed on a polycrystalline platinum surface. Under conditions where the reaction rate is linearly dependent on ammonia pressure, the observed activation energy is 1 ± 1 kcal/mol. For conditions where the rate of decomposition becomes independent of ammonia pressure, the observed activation energy increases to 24 ± 4 kcal/mol.

2. Nitrogen adatoms are the predominant surface species during ammonia decomposition at 2 × 10^{-6} Torr. For temperatures below 400 K, the Pt(110)-(1 × 2) surface is saturated with nitrogen adatoms. At higher temperatures, the fractional coverage of nitrogen adatoms decreases, becoming <0.1 for temperatures above 600 K.

3. The mechanistic model developed previously for the decomposition of ammonia on a polycrystalline platinum wire[3] describes accurately the pressure and temperature dependence of the reaction rate and the measured steady-state coverage of nitrogen adatoms on the Pt(110)-(1 × 2) surface.

4. The recombinative desorption of nitrogen is the major reaction mechanism producing molecular nitrogen during ammonia decomposition at 2 × 10^{-6} Torr.

Acknowledgment. This research was supported by the National Science Foundation under Grant No. CHE-8516615.

Thermodynamics of Proton Transfer in Phenol–Acetate Hydrogen Bonds with Large Proton Polarizability and the Conversion of Light Energy into Chemical Energy in Bacteriorhodopsin

Helmut Merz, Ulrike Tangermann, and Georg Zundel*

Institut für Physikalische Chemie der Universität München, D-8000 München 2, FRG
(Received: December 30, 1985)

Phenol–acetate solutions in CCl_4 are studied by IR spectroscopy as a function of the pK_a of the phenols. The (I) Ar–OH···$^-$OC ⇌ Ar–O$^-$···HOC (II) hydrogen bonds formed show large proton polarizability as indicated by continua in the IR spectra. The percent proton transfer (PT) increases from the *p*-cresol–acetate to the pentachlorophenol–acetate system from 0% to 56%. The Gibbs free energy, $\Delta G°_{PT}$, values of the PT equilibria at 295 K are determined as well as the standard enthalpy values, $\Delta H°_{PT}$, and the standard entropy values, $\Delta S°_{PT}$. These data are given in Table II. The shape of the intensity of the continuum as a function of the $\Delta H°_{PT}$ value changes. In the classical approximation the average difference between the two minima of the proton double-minimum potential is given by $\Delta H°_{PT}$. With the decreasing amount of $\Delta H°_{PT}$, i.e., decreasing degree of asymmetry, the intensity of the continua decreases at higher and increases at lower wavenumbers. This result is in good agreement with the predictions from calculated line spectra. In the photocycle of bacteriorhodopsin a tyrosine–aspartate hydrogen bond is probably of importance for the conversion of light energy into chemical energy. On the basis of the obtained data it is shown that 9.5 kJ/mol can be converted into chemical energy due to a proton transfer induced by a local electrical field in a Tyr–Asp hydrogen bond. Furthermore, if the Ar–O$^-$···HOC structure is broken afterwards by a conformational change, at least 25 kJ/mol of conformational energy is converted. Thus, altogether 34.5 kJ/mol of Gibbs free energy may be converted into chemical energy and stored by these processes.

Introduction

Hydrogen bonds with a double-minimum proton potential show large proton polarizability; that means that the proton can easily be shifted by a local electrical field within these hydrogen bonds.[1,2] The presence of such hydrogen bonds is indicated by continua in the infrared spectra.[3–5] In the case of OH···O$^-$ ⇌ $^-$O···HO bonds with an O–O distance of 2.6–2.65 Å, the wavenumber dependence of the intensity of the continua is expected to be a function of the degree of asymmetry of the double-minimum proton potential.[2,6] In the classical approximation, $\Delta H°_{PT}$, the enthalpy of the proton-transfer reaction in a AH···B$^-$ ⇌ A$^-$···HB bond, is the energy difference between the minima of the double-minimum proton potential. Caused by the large proton polarizability, the shape of the proton potentials of such hydrogen bonds in solutions shows a distribution. Hence, measured $\Delta H°_{PT}$ values are the average energy differences of the two minima. To check whether the

(1) Weidemann, E. G.; Zundel, G. *Z. Naturforsch., A* **1970**, *25A*, 627.
(2) Janoschek, R.; Weidemann, E. G.; Pfeiffer, H.; Zundel, G. *J. Am. Chem. Soc.* **1972**, *94*, 2387.
(3) Zundel G. In *The Hydrogen Bonds—Recent Developments in Theory and Experiments*; Schuster, P., Zundel, G., Sandorfy, C., Eds.; North Holland: Amsterdam, 1976; Vol. II, Chapter 15, p 681.
(4) Lindemann, R.; Zundel, G. *J. Chem. Soc., Faraday Trans. 2* **1977**, *73*, 788.
(5) Zundel, G. In *Biophysics*; Hoppe, W., Lohmann, W., Markl, H., Ziegler, H., Eds.; Springer: Berlin, 1983; pp 143–154.
(6) Janoschek, R.; Weidemann, E. G.; Zundel, G. *J. Chem. Soc., Faraday Trans. 2* **1973**, *69*, 505.

0022-3654/86/2090-6535$01.50/0

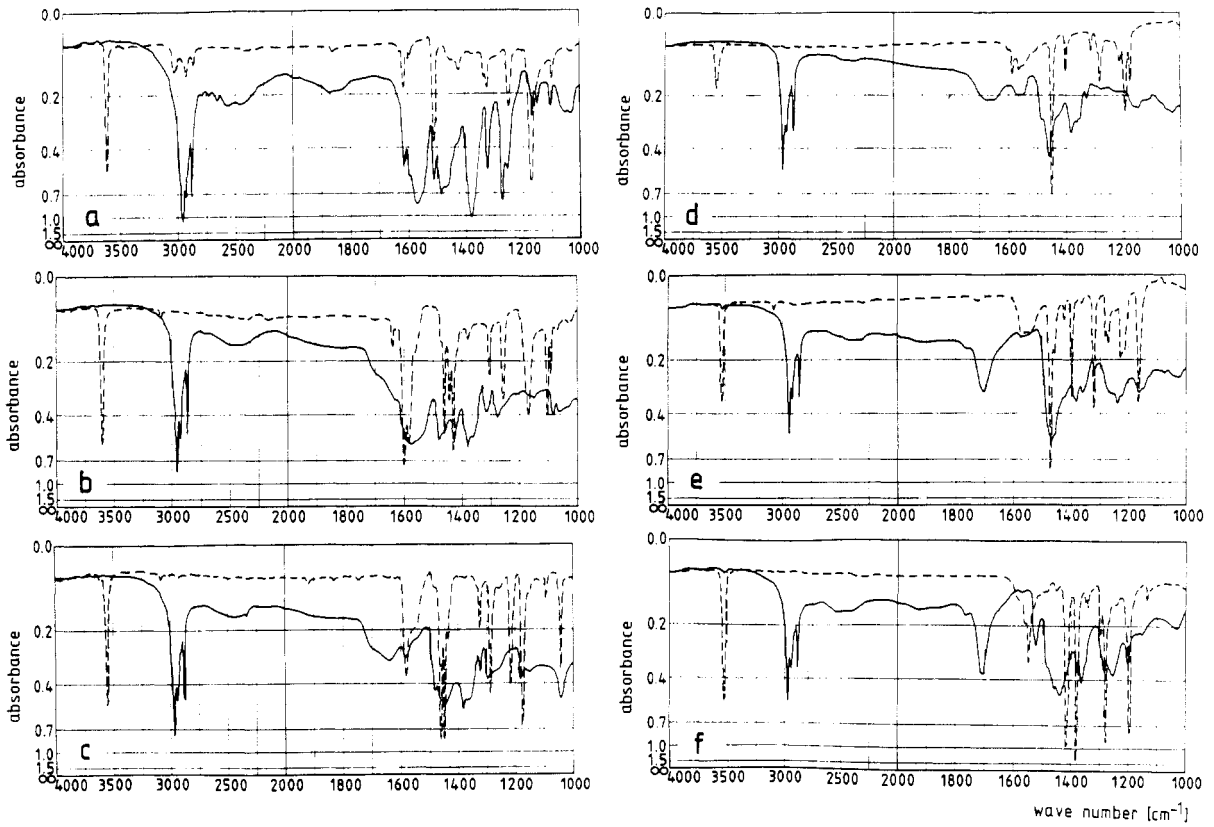

Figure 1. IR spectra of phenols (- - -) and of the corresponding phenol + tetrabutylammonium acetate systems (—) in CCl_4 at 295 K. Layer thickness is 528 μm except in the case of pure 2,3,4-TCP (d) where it is 127 μm. For abbreviations of phenols, see Table III. (a) *p*-cresol, c = 0.029 mol/L, *p*-cresol + TBAA, c = 0.037 mol/L; (b) 3,5-DCP, c = 0.040 mol/L, 3,5-DCP + TBAA, c = 0.030 mol/L; (c) 2,3-DCP, c = 0.039 mol/L, 2,3-DCP + TBAA, c = 0.031 mol/L; (d) 2,3,4-TCP, c = 0.054 mol/L, 2,3,4-TCP + TBAA, c = 0.020 mol/L; (e) 2,4,6-TCP, c = 0.020 mol/L, 2,4,6-TCP + TBAA, c = 0.020 mol/L; (f) PCP, c = 0.030 mol/L, PCP + TBAA, c = 0.020 mol/L.

above-mentioned theoretical predictions are true, we studied Ar–OH···$^-$OC ⇌ Ar–O$^-$···HOC hydrogen bonds in phenol–acetate systems with regard to the shape of the continua and the thermodynamic quantities.

A second reason to perform these studies was the problem of how in the case of bacteriorhodopsin light energy is converted into electrochemical energy. Bacteriorhodopsin (BR) is the main protein component of the purple membrane of halobacteria. Upon illumination a photocycle is initiated in BR. During this photocycle, this protein pumps protons across the purple membrane, thus converting light energy into electrochemical energy.[7-9] In the microsecond time range of this photocycle, a tyrosine residue is deprotonated. Slightly different times are given by the various authors.[10-12] In the same time range at least two aspartate residues are protonated.[13-16] These results taken together suggest that a proton transfer occurs in a Tyr–Asp hydrogen bond. On the basis of the data presented in this publication, the role that this Tyr–Asp hydrogen bond may play with the conversion of the light energy into electrochemical energy is discussed, and the thermodynamic quantities of these processes can be estimated. Herewith, the transfer of the proton in the hydrogen bond with large proton polarizability due to a change of the local electrical field, as well as the breaking of this hydrogen bond afterwards, may be important with regard to the conversion of light energy into chemical energy and the storage of this energy. Such a mechanism seems reasonable since the local electrical fields in the active center of BR change fundamentally[17,18] and since due to a trans–cis isomerization of the retinal residue[19,20] considerably sterical changes may occur during the photocycle.

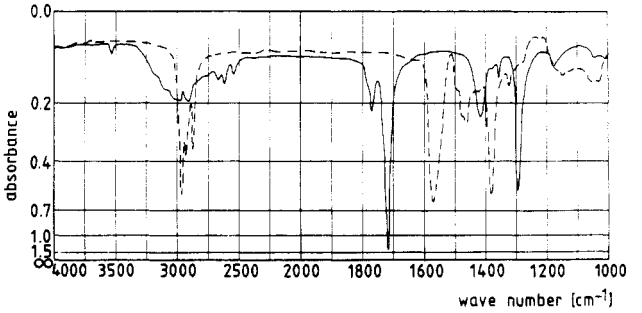

Figure 2. IR spectra of (—) acetic acid, 0.040 mol/L in CCl_4, and (- - -) tetrabutylammonium acetate, 0.019 mol/L in CCl_4.

Results and Discussion

Figure 1 shows spectra of CCl_4 solutions of phenol–acetate systems together with the spectra of the pure phenols, whereby the pK_a of the phenols decreases from the system shown in Figure 1a to that shown in Figure 1f. In Figure 2 the spectra of the pure tetrabutylammonium acetate and of the pure acetic acid solutions are shown for comparison. ν_{OH} of the pure phenol is found as a narrow band in the region 3500–3600 cm^{-1}. This band vanishes

(7) Oesterhelt, D.; Stoeckenius, W. *Nature (London), New Biol.* **1971**, *233*, 149.
(8) Stoeckenius, W.; Bogomolni, R. A. *Ann. Rev. Biochem.* **1982**, *52*, 587.
(9) Bamberg, E.; Apell, H.-J.; Dencher, N. A.; Sperling, W.; Stieve, H.; Läuger, P. *Biophys. Struct. Mech.* **1979**, *5*, 277.
(10) Hess, B.; Kuschmitz, D. *FEBS Lett.* **1979**, *100*, 334.
(11) Hanamoto, J. H.; Dupuis, P.; El-Sayed, H. A. *Proc. Natl. Acad. Sci. U.S.A.* **1984**, *81*, 7083.
(12) Dupuis, P.; El-Sayed, M. A. *Can. J. Chem.* **1985**, *63*, 1699.
(13) Rothschild, K. J.; Zagaeski, M.; Cantore, W. A. *Biochem. Biophys. Res. Commun.* **1981**, *103*, 483.
(14) Bagley, K.; Dollinger, G.; Eisenstein, L.; Singh, A. K.; Zimanyi, L. *Proc. Natl. Acad. Sci. U.S.A.* **1982**, *79*, 4972.
(15) Siebert, F.; Mäntele, W.; Kreutz, H. *FEBS Lett.* **1982**, *141*, 82.
(16) Engelhard, M.; Gerwert, K.; Hess, B.; Siebert, F. *Biochemistry* **1985**, *24*, 400.
(17) Warshel, A. *Photochem. Photobiol.* **1979**, *30*, 285.
(18) Honig, B. *Current Top. Membranes Transp.* **1982**, *16*, 371.
(19) Tsuda, M.; Glaccum, M.; Nelson, B.; Ebrey, T. G. *Nature (London)* **1980**, *287*, 351.
(20) Kuschmitz, D.; Hess, B. *FEBS Lett.* **1982**, *138*, 137.

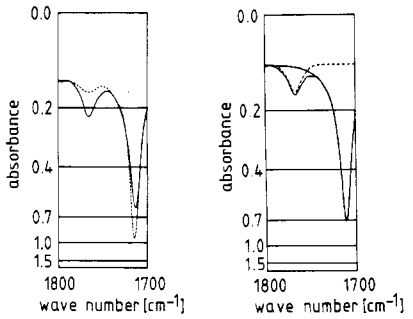

Figure 3. (a, left) IR spectra of acetic acid, 0.020 mol/L in CCl_4, at T = 312 K (—) and at T = 264 K (---). (b, right) Band separation of an IR spectrum of acetic acid, 0.020 mol/L in CCl_4, at 295 K. Left band, $\nu_{C=O}$ of the monomer; right bands, $\nu_{C=O}$ of the dimer.

almost completely with the addition of the acetate, indicating hydrogen bond formation. In Figure 2 $\nu_{C=O}$ of the acid is found at 1765 cm^{-1} (monomers) and at 1715 cm^{-1} (dimers). Respective bands are found in the spectra of the phenol + acetate solutions, whereby the latter band is masked by the $\nu_{C=O}$ vibration of the hydrogen-bonded complex. These bands are not present in the spectrum of Figure 1a since in the *p*-cresol–acetate system the proton is located at the phenolic group. In the series of complexes from Figure 1b to Figure 1f these bands increase since the degree of proton transfer from the phenol to the acetate increases. Correspondingly the ν_{as,CO_2^-} vibration at about 1650 cm^{-1} decreases. (In the pure tetrabutylammonium acetate (Figure 3) and if the hydrogen bonds are weak (Figure 1a), this band appears below 1600 cm^{-1}; it is shifted toward higher wavenumbers with increasing strength of the hydrogen bond (see Figure 1b–1e).)

These bands show that both proton-limiting structures Ar–O-H···$^-$OOCCH$_3$ ⇌ Ar–O$^-$···HOOCCH$_3$ can be distinguished in the infrared spectra. The result that the bands of both structures are observed in the spectra demonstrates that the proton potential in these hydrogen bonds is a double-minimum potential.

The following equilibria have to be considered:

hydrogen bond formation

$$\text{Ar–OH} + {}^-\text{OOC–CH}_3 \overset{K_b}{\rightleftharpoons} \text{Ar–OH···}{}^-\text{OOCCH}_3$$

proton transfer (PT)

$$\text{Ar–OH···}{}^-\text{OOCCH}_3 \overset{K_{PT}}{\rightleftharpoons} \text{Ar–O}^-\text{···HOOCH}_3$$

hydrogen bond dissociation

$$\text{Ar–O}^-\text{···HOOCH}_3 \overset{K_{dis}}{\rightleftharpoons} \text{Ar–O}^- + \text{HOOCH}_3$$

dimerization

$$2\text{CH}_3\text{COOH} \overset{K_{dim}}{\rightleftharpoons} (\text{CH}_3\text{COOH})_2$$

In order to determine the PT equilibrium constant, K_{PT}, the concentrations of the left Ar–OH···$^-$OOCCH$_3$ and the right Ar–O$^-$···HOOCH$_3$ proton-limiting structure have to be determined.

The left proton-limiting structure can be determined from the integral absorbance of the ν_{as,COO^-} band which appears in the range 1580–1650 cm^{-1}. This band is calibrated by using the respective band of the pure tetrabutylammonium acetate solution. Herewith the contribution of the free acetate can be neglected since the first equilibrium is almost completely shifted to the right as shown by the fact that the ν_{OH} vibration of the free phenols is, whenever observed, only a very weak band.

Furthermore, the concentrations of the left proton-limiting structure can be determined in a second way: For the initial concentration of acetate (c_{OA})

$$c_{OA} = c_M + 2c_D + c_L + c_R + c_{A^-}$$

holds. Herewith c_M and c_D are the concentrations of monomeric and dimeric acetic acid, respectively, c_L and c_R are the concentrations of left and right proton-limiting structures, and c_{A^-} is the concentration of non-hydrogen-bonded acetate. As described above, the latter concentration may be neglected. Thus, one obtains

$$c_L = c_{OA} - c_M - 2c_D - c_R$$

for c_L. The initial concentration of acetate is known; c_M, c_D, and c_R can be determined as described below. The results of both calculations of c_L were in very good agreement.

The right proton-limiting structure is obtained from $\nu_{C=O}$ at about 1700 cm^{-1}. From the absorbance of this band the contribution of the dimeric acetic acid must be subtracted. This contribution is obtained from $\nu_{C=O}$ of the monomers at 1765 cm^{-1} and from the dimerization constant K_{dim}.

This dimerization constant as well as the absorptivity constant of $\nu_{C=O}$ of the monomers and dimers was determined as follows:

Spectra of pure acetic acid solutions (0.020 mol/L) in CCl_4 were taken at various temperatures (Figure 3a). The integrated absorbances of the monomer, E_m, and the dimer, E_D, bands were determined by using a band separation program[21] (Figure 3b). For the evaluation, the eq 1–3 were used.

$$E_M = c_M \epsilon_M d \quad (1)$$

$$E_D = c_D \epsilon_D d \quad (2)$$

$$c_0 = c_M + 2c_D \quad (3)$$

Herewith ϵ_M and ϵ_D are the absorptivity coefficients, d is the layer thickness, and c_0 is the initial concentration of the acid. From these equations, eq 4 is obtained. Thus, there is a linear relation

$$E_M = -2E_D\frac{\epsilon_M}{\epsilon_D} + \epsilon_M c_0 d \quad (4)$$

between E_M and E_D for various temperatures. From this relation ϵ_M and ϵ_D are obtained by linear regression. Now, one obtains c_M and c_D by using eq 1 and 2. The dimerization constant K_{dim} is given by eq 5 and is obtained in this way for the various temperatures (Table I).

$$K_{dim} = \frac{c_D}{c_M^2} \quad (5)$$

Figure 4 shows ln K_{dim} as a function of $1/T$. According to van't Hoff

$$\ln K = -\frac{\Delta H^\circ}{RT} + \frac{\Delta S^\circ}{R} \quad (6)$$

TABLE I: Dimerization Constant of Acetic Acid, 0.020 mol/L in CCl_4, at Various Temperatures

	T, K				
	332	323	315	298	284
K_{dim}, L/mol	735	1130	1510	4900	12 100

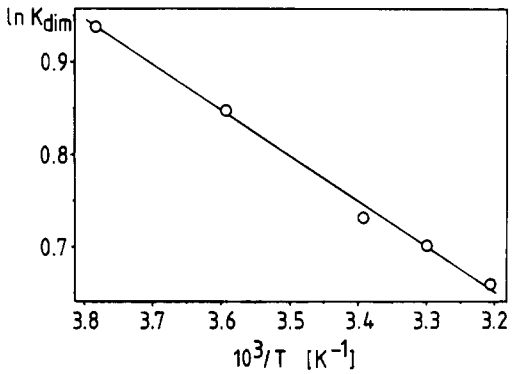

Figure 4. ln K_{dim} of acetic acid, 0.020 mol/L in CCl_4, as a function of reciprocal temperature (van't Hoff plot).

(21) Jones, P. N., et al. *Nat. Res. Counc. Can. Bull.* **1968**, *11*, 12; **1969**, *11*, 13.

TABLE II: Thermodynamic Data of the Phenol–Acetate Systems. $\Delta H°_{PT}$ and $\Delta S°_{PT}$ Values of Systems 1–6 Were Determined by Extrapolation (See Figure 7) as well as $\Delta G°_{PT}$ of System 1 (Figure 6b)

phenol	ΔpK_a	% PT[a]	$\Delta G°_{PT}$,[a] kJ/mol	$\Delta H°_{PT}$, kJ/mol	$\lvert\Delta H°_{PT}/(hcN)\rvert$, cm^{-1}	$\Delta S°_{PT}$, J/(mol K)
1, *p*-cresol	5.42	0	9.5	8	670	5
2, 3,5-DCP	3.49	8	6.1	2	170	12
3, 2,4-DCP	3.14	9	5.7	1	80	13
4, 2,3-DCP	2.95	15	4.2	1	80	13
5, 2,3,4-TCP	2.21	18	3.6	−1	80	15
6, 2,4,5-TCP	1.96	19	3.5	−2	170	16
7, 2,3,5-TCP	1.67	25	2.6	−2	170	16
8, 2,4,6-TCP	1.23	33	1.8	−4	330	20
9, PCP	−0.02	56	−0.6	−7	590	22

[a] At 295 K.

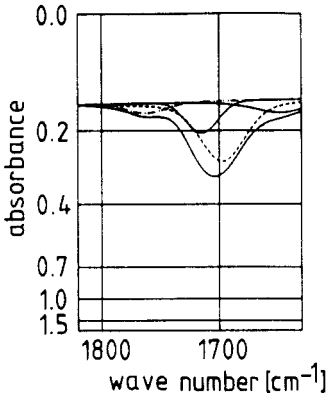

Figure 5. Band separation of an IR spectrum of 2,4,6-trichlorophenol + tetrabutylammonium acetate, 0.020 mol/L in CCl_4, at T = 295 K. The bands into which this part of the spectrum is separated are (from left to right) $\nu_{C=O}$ of monomeric and dimeric acetic acid, $\nu_{C=O}$ of acetic acid hydrogen bonded to the phenol, and ν_{as,CO_2^-} of hydrogen-bonded acetate.

the thermodynamic quantities for the dimerization of acetic acid in CCl_4 are obtained. They are $\Delta H°_{dim}$ = −41 kJ/mol and $\Delta S°_{dim}$ = −77 J/(mol K).

The concentrations of the various species in the phenol–acetate systems were determined by a separation of the various carboxylic acids and carboxylate bands in the spectra of the mixtures using the band separation program.[21] Examples are shown in Figure 5.

As described above, from these integrated absorbances the percent proton transfer (% Pt) and K_{PT} are obtained according to eq 7. The % PT and $\Delta G°_{PT}$ at 295 K are given in Table II

$$K_{PT} = c_R/c_L \qquad PT = \frac{c_R}{c_L + c_R}100 \tag{7}$$

for the various systems. In Figure 6a the % PT are shown as a function of the ΔpK_a, i.e., the pK_a of the acetic acid minus that of the phenols. In Figure 6b $\Delta G°_{PT}$ is shown as a function of the ΔpK_a. According to Huyskens, $\Delta G°_{PT}$ decreases in proportion to ΔpK_a. Huyskens[22,23] postulated that eq 8 is valid for a family of systems. Such a family is characterized as follows.[22,23] In a

$$\log K_{PT} = -\frac{\Delta G°_{PT}}{2.3RT} = \xi\Delta pK_a - \delta \tag{8}$$

family of systems the chemical compounds possess the same donor or acceptor groups. These compounds have, however, different pK_a values due to different substituents, but these substituents show similar interaction properties with their environments. In the case of the phenol–acetate systems in CCl_4 the following values are obtained from Figure 6b: ξ = 0.32, δ = 0.08, and $\Delta pK_a^{50\%}$ = 0.24 (value for K_{PT} = 1). By using tetrabutylammonium as the cation in these systems, the influence of the counterion on the charged hydrogen bond was minimized. Tetrabutylammonium is a rather large and soft cation with extremely little polarizing power (Figure 2c in ref 23b).

In the case of three phenol + acetate systems, it was possible to determine $\Delta H°_{PT}$ and $\Delta S°_{PT}$ from a study of the equilibria as a function of the temperature.

These values could only be measured for the systems in which $\Delta H°_{PT}$ is negative and its amount large enough. If $\Delta H°_{PT}$ is near zero, the changes of K_{PT} with temperature are too small. On the

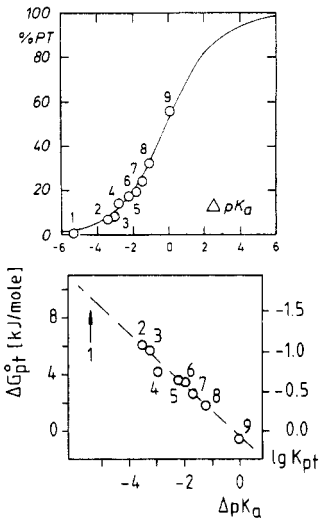

Figure 6. (a, top) Degree of proton transfer in the phenol–acetate systems as a function of the ΔpK_a (i.e., pK_a of acetic acid minus pK_a of the phenol) at 295 K. The numbers indicate the phenols used (see Table II). (b, bottom) $\Delta G°_{PT}$ or log K_{PT} in the phenol–acetate systems as a function of ΔpK_a (Huyskens plot) at 295 K. The arrow indicates the place where the value for the *p*-cresol–acetate system is to be expected.

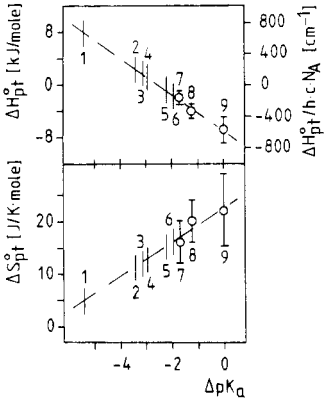

Figure 7. $\Delta H°_{PT}$ and $\Delta S°_{PT}$ in the phenol–acetate systems as a function of the ΔpK_a. (O) measured data; (|) places where the values for the systems that could not be detemrined experimentally are to be expected. Numbers correspond to the systems given in Table II.

(22) Huyskens, P.; Zeegers-Huyskens, Th. *J. Chim. Phys.* **1964**, *61*, 81.
(23) (a) Zeegers-Huyskens, T.; Huyskens, P. In *Molecular Interaction*; Ratajczak, H., and Orville-Thomas, W. J., Eds.; Wiley: New York, 1980; Vol. 2, pp 1–106. (b) Schiöberg, D.; Zundel, G. *Can. J. Chem.* **1976**, *54*, 2193.

other hand, if $\Delta H°_{PT}$ is positive, i.e., the equilibrium is on the left-hand side, a change of the equilibrium could only be expected if the solutions are heated; however, under these conditions the hydrogen bonds break.

In Figure 7 these values are shown as a function of the ΔpK_a. The dashed lines are extrpolations under the assumption that $\Delta H°_{PT}$ and $\Delta S°_{PT}$ change in proportion to the ΔpK_a analogously to $\Delta G°_{PT}$ (Huyskens relation[22,23]). In this way extrapolated $\Delta H°_{PT}$ and $\Delta S°_{PT}$ values are obtained, also for the systems with which these values cannot be measured directly. The directly measured as well as the extrapolated $\Delta H°_{PT}$ and $\Delta S°_{PT}$ values are given in Table II.

The errors in the determination of $\Delta H°_{PT}$ and $\Delta S°_{PT}$ are considerably larger than in the determination of $\Delta G°_{PT}$ which is indicated by error bars in Figure 7. The error in determining $\Delta G°_{PT}$ is directly related to errors in the IR-spectroscopic determination of concentrations. Herewith the most significant errors arise from nonideal band separation, especially when more than two bands overlap. This is no problem, for example, with the determination of K_{dim} of acetic acid, as there two already well-separated bands are present which can be integrated rather exactly. On the other hand, with the systems shown in Figure 1 four bands have to be separated (see Figure 5) which overlap strongly. In such cases, the result of the curve-fitting process is to a certain degree dependent on the starting parameters the band separation program is supplied with. By varying these parameters we estimated the errors made in the determination of the concentrations. Depending on the system investigated, the relative error is in the range 5–20%. For calculation of $\Delta G°_{PT}$ the logarithm of a quotient of such concentration values has to be taken. Herewith an error in $\Delta G°_{PT}$ results which is less than 1 kJ/mol in the case of all systems studied quantitatively. For the relation between $\Delta G°_{PT}$ at two different temperatures and $\Delta H°_{PT}$ the equation

$$\Delta H°_{PT} = \Delta G°_{PT}(1)\frac{T(1)}{T(2) - T(1)} - \Delta G°_{PT}(2)\frac{T(2)}{T(2) - T(1)}$$

holds. This equation shows that the errors in determining $\Delta H°_{PT}$ are significantly larger than the errors for $\Delta G°_{PT}$. An analogous consideration holds for $\Delta S°_{PT}$. Corresponding error estimates are indicated by the error bars in Figure 7.

Figure 1a–1f shows that in all systems IR continua are observed. They demonstrate that in all systems the Ar–OH···$^-$OC ⇌ Ar–O$^-$···HOC bonds show large proton polarizability. The shape of the continua shows, however, a characteristic change within this series of systems. In the cases of the *p*-cresol + acetate (Figure 1a) and the pentachlorophenol + acetate (Figure 1f) systems, the continua begin at about 3000 cm^{-1} and extend toward smaller wavenumbers. Except for two less pronounced maxima at about 2600 and 1900 cm^{-1}, the intensity is independent of the wavenumber in the whole region studied. In the cases of 3,5-dichlorophenol + acetate (Figure 1b) and the 2,4,6-trichlorophenol + acetate (Figure 1e) systems, the intensity of the continuum decreases slightly at higher wavenumbers and increases at lower wavenumbers. Finally, in the 2,3-dichlorophenol + acetate system (Figure 1c) and in the 2,3,4-trichlorophenol + acetate system (Figure 1d), the intensity of the continuum decreases even more at higher wavenumbers and increases strongly at smaller wavenumbers. Thus, with increasing ΔpK_a, first, the intensity of the continuum decreases at higher wavenumbers and increases at lower wavenumbers; if the ΔpK_a increases further, the opposite is true.

This change of the shape of the continuum is correlated with the change of the $\Delta H°_{PT}$ values (Table II, column 6). In the classical approximation $\Delta H°_{PT}$ is the difference of the two minima of the double-minimum potential. In real systems the shape of the proton potential shows a distribution since, caused by the local fields in the solutions, hydrogen bonds with large proton polarizability are more or less strongly polarized. Hence, in the classical approximation the obtained $\Delta H°_{PT}$ values are the average differences of the two minima of the proton potentials. The theory of hydrogen bonds with large proton polarizability, developed using $H_5O_2^+$ as an example,[2,6] shows—in the case of O–O distances 2.60–2.65 which may roughly correspond to the O–O distance of our system—the following: with decreasing degree of asymmetry of the proton potentials (Figure 5 in ref 2) the line spectra (Figure 6 in ref 6 or Figure 7 in ref 24a) show that the maximum of the intensity distribution shifts toward smaller wavenumbers. In the theoretical calculations, increasing degree of asymmetry of the proton potential is induced by an electrical field. Decreasing field strength corresponds to a decreasing degree of asymmetry (see Figure 5 in ref 2).

In the systems with positive $\Delta H°_{PT}$ values, the deeper well of the double minimum is on the left-hand side and in those with negative $\Delta H°_{PT}$ values is on the right-hand side. Figure 1 and the $\Delta H°_{PT}$ values in Table II, column 6, show that with charged hydrogen bonds the intensity distribution of the continuum is the same for positive and negative $\Delta H°_{PT}$ values if their amounts are equal. Furthermore, with a decreasing amount of $\Delta H°_{PT}$, i.e., decreasing degree of asymmetry of the proton potential, in the phenol–acetate systems the intensity of the continuum decreases at higher wavenumbers and increases at lower wavenumbers.

Thus, the wavenumber distribution of the intensity of the continuum in the series of systems in Figure 1 is in good agreement with the change of the degree of asymmetry of the proton potentials, given by the determined $\Delta H°_{PT}$ values (Table II, columns 6 and 7).

Energetics of the Tyrosine–Aspartate Hydrogen Bond in Bacteriorhodopsin. During the photocycle of bacteriorhodopsin, a tyrosine residue is deprotonated and various aspartate residues are protonated and deprotonated.[10–16] Roughly parallel to the deprotonation of the tyrosine, one of these aspartate groups is protonated at about 60 μs after the start of the photocycle.[13–16] These results suggest that a transfer of a proton in a tyrosine–aspartate hydrogen bond is involved in the conversion of light energy into chemical energy.

There is no direct experimental evidence for the existence of a Tyr–Asp hydrogen bond in BR, but there are some observations which strongly suggest that such a hydrogen bond is present: Firstly, there is a close spatial relationship between a tyrosine and an aspartate residue in BR. It is known from the primary structure of BR that Asp-212 is near the chromophore. Chemical modifications[24b] of tyrosine have shown that Tyr-26 is near the chromophore, too. Secondly, there are corresponding protonation changes in a similar time range. Deprotonation of tyrosine and protonation of aspartate are correlated.[10–16] It seems to be a reasonable suggestion that there is a direct proton transfer from tyrosine to aspartate which will only proceed via a hydrogen bond. It cannot be ruled out, of course, that the protonation changes reflect proton transfers to other groups or a proton transfer from tyrosine to aspartate via such groups. Our model systems were chosen to represent the interior of a membrane protein as closely as possible with such simple molecules. CCl_4 has a similar dielectric permittivity as the interior of biological membranes, so the overall influence of the environment should be similar in the model systems. Of course, it is not possible to take into account specific interactions with such model systems.

The system *p*-cresol + acetate (system 1) corresponds to the tyrosine–aspartate hydrogen bond since the side chain of tyrosine is chemially analogous to *p*-cresol and that of aspartic acid to acetic acid. The ΔpK_a values of both systems are similar.

Figure 6a shows that in the *p*-cresol–acetate system (system 1) the proton in the Ar–OH···$^-$OC ⇌ Ar–O$^-$···HOC bonds is almost completely localized at the phenolic group. The continuum in the spectrum of this system demonstrates (Figure 1f) that the hydrogen bond in this complex shows proton polarizability; hence the positive charge can easily be shifted by an electrical field from the phenol to the carboxylate group.

Columns 5 and 6 in Table II, respectively, show that the standard enthalpy $\Delta H°_{PT}$ of the proton transfer reaction in this system amounts to +8 kJ/mol and the Gibbs free energy $\Delta G°_{PT}$ at 295 K amounts to +9.5 kJ/mol. Thus, if the proton is shifted by an electrical field in this hydrogen bond from the phenolic to

(24) (a) Böhner, U.; Zundel, G. *J. Phys. Chem.* **1986**, *90*, 964. (b) Lemke, H. D.; Oesterhelt, D. *Eur. J. Biochem.* **1981**, *115*, 595.

TABLE III: List of Phenols Used

phenol	abbrev	purchased from	quality	pK_a	ref
1, *p*-cresol		Fluka	puriss.	10.18	26
2, 3,5-dichlorophenol	3,5-DCP	Aldrich	99%	8.25	27
3, 2,4-dichlorophenol	2,4-DCP	Aldrich	98%	7.90	27
4, 2,3-dichlorophenol	2,3-DCP	Fluka	purum	7.71	27
5, 2,3,4-trichlorophenol	2,3,4-TCP	Aldrich	97%	6.97	27
6, 2,4,5-trichlorophenol	2,4,5-TCP	Aldrich	99%	6.72	27
7, 2,3,5-trichlorophenol	2,3,5-TCP	Fluka	puriss.	6.43	27
8, 2,4,6-trichlorophenol	2,4,6-TCP	Aldrich	98%	5.99	27
9, pentachlorophenol	PCP	Fluka	puriss.	4.74	27

the carboxylate group, 9.5 kJ/mol is converted from electrical into chemical energy.

After the transfer of the proton to the aspartate group, the hydrogen bond has to be broken. This hypothesis is confirmed by the experimental results that two carboxylic acid groups arising during the photocycle are not hydrogen bonded.[13-16] This breaking of the Tyr–Asp hydrogen bond has two consequences. Firstly, the energy of the field-induced proton transfer in the Tyr–Asp bond is stored, since the proton cannot return to the tyrosine. Secondly, since the hydrogen bond is probably broken by a conformational constraint in the active site, additional Gibbs free energy, the Gibbs free energy necessary for breaking the hydrogen bond, is converted into chemical energy and stored. This energy contribution arises from conformational energy.

From our measurements the amount of this contribution can be estimated since it is possible to estimate the thermodynamic quantities of the hydrogen bond dissociation reaction $Ar–O^-\cdots HOC \rightleftharpoons Ar–O^- + HOC$.

In the case of the pentachlorophenol + acetate system (Figure 1f), these data can be directly determined. The concentrations of $Ar–O^-\cdots HOC$ and of the monomeric acetic acid (HOC) have been determined with the calculation of the proton-transfer equilibrium. The concentration of the free phenolate ($Ar–O^-$) is equal to the sum of the non-hydrogen-bonded monomeric and of the dimeric carboxylic acid. Both concentrations are already known. From these data $\Delta G°_{dis}$ of the dissociation of the $Ar–O^-\cdots HOC$ hydrogen bond is obtained; it amounts to 25 kJ/mol at 295 K.

Furthermore, Figure 1 shows that the formation constant, K_b, of the left proton-limiting structure $Ar–OH\cdots{}^-OC$ is obtained from the ν_{OH} band of the non-hydrogen-bonded OH groups at about 3550 cm^{-1} in the spectra of the phenol–acetate systems. Whenever such a band is observed in these spectra, the concentration of free phenol can be estimated by comparison of the integrated absorbance of this hand with the respective band of the free phenol. This estimation shows that in all systems K_b is larger than 9×10^4 L mol^{-1}. Thus, the amount of the negative $\Delta G°_b$ value at 295 K of the nonpolar structure is larger than 28 kJ/mol.

Both estimations show that the Gibbs free energy of formation of such hydrogen bonds in CCl_4 amounts to at least 25 kJ/mol. Hence, this amount of Gibbs free energy is necessary to break such a hydrogen bond. In the case of bacteriorhodopsin the source of this energy can only be conformational energy.

Thus, if the Tyr–Asp bond is broken an additional amount of Gibbs free energy of at least 25 kJ/mol is converted from conformational energy resulting from light energy—probably due to the conformational change of the retinal residue—into chemical energy and stored. Thus, caused by the field-induced proton transfer in the $Ar–OH\cdots{}^-OC \rightleftharpoons Ar–O^-\cdots HOC$ hydrogen bond and by the breaking of the $Ar–O^-\cdots HOC$ proton-limiting structure of this bond altogether, at least 34.5 kJ/mol of Gibbs free energy is converted into chemical energy and stored.

Conclusions

The position of the proton-transfer (PT) equilibria in (I) $Ar–OH\cdots{}^-OC \rightleftharpoons Ar–O^-\cdots HOC$ (II) bonds are determined, formed between phenols and acetate in CCl_4 solutions. The percent proton transfer as a function of the ΔpK_a is shown in Figure 6a, whereas Figure 6b shows $\Delta G°_{PT}$ as a function of the ΔpK_a (Huyskens plot). The % PT increases from the *p*-cresol–acetate to the pentachlorophenol–acetate system from 0% to 56%. In the case of the PCP–acetate, 2,4,6-trichlorophenol–acetate, and 2,3,5-trichlorophenol–acetate systems, the standard enthalpy $\Delta H°_{PT}$ and the standard entropy $\Delta S°_{PT}$ of the transfer reactions are obtained from the temperature dependence of the PT equilibria. Under the assumption that the Huyskens relation is also valid in the case of these quantities, for the other systems extrapolated values are obtained (Figure 7). All these thermodynamic data of the PT equilibria are summarized in Table II.

In the case of all these systems, a continuum indicates that the proton may fluctuate within these H bonds and these H bonds show large proton polarizability. The intensity of these continua as a function of the wavenumbers shows a characteristic change as a function of $\Delta H°_{PT}$. In the classical approximation $\Delta H°_{PT}$ gives the average difference between the two minima of the double-minimum proton potential. From the *p*-cresol–acetate to pentachlorophenol–acetate systems, the deeper well shifts from the phenol to the acetate. If $\Delta H°_{PT}$ is positive or negative and its amount is large, the continua begin at 3000 cm^{-1} and extend with almost the same intensity over the whole region. If the amount of $\Delta H°_{PT}$ becomes smaller, the intensity of the continua decreases at higher wavenumbers and increases strongly at lower wave numbers, i.e., the shape of the intensity of the continuum as a function of the wavenumber changes in the same way in the case of positive and negative $\Delta H°_{PT}$ values if the degree of asymmetry of the proton potential decreases. This behavior as a function of the degree of asymmetry of the proton potential is predicted from calculated line spectra.

Light energy is converted into electrochemical energy by the bacteriorhodopsin molecule in the purple membrane of halobacteria. This is performed by a photocycle in which protons are pumped from the inside to the outside of the membrane. In one step of this cycle, a tyrosine–aspartate hydrogen bond is of particular significance. Our data show that if a local field shifts the proton from the Tyr to the Asp residue, 9.5 kJ/mol is converted from electrical into chemical energy. If this hydrogen bond is broken after the PT due to a conformational change, at least additional 25 kJ/mol is converted from conformational into chemical energy. This conformational energy may arise by the light-induced conformational change of the retinal residue. Thus, caused by the field-induced proton transfer in a Tyr–Asp hydrogen bond and by the breaking of the $Ar–O^-\cdots HOC$ proton-limiting structure of this bond altogether, at least 34.5 kJ/mol of Gibbs free energy is converted into chemical energy and stored.

Experimental Section

Substances. Tetrabutylammonium acetate was purchased from Fluka. It contained traces of HCO_3^- and water that had to be removed before use. HCO_3^- was replaced by acetate by using an anion exchanger loaded with sodium acetate. Only water that had been made CO_2-free by extensive boiling was used for this ion-exchange procedure. Thus, a carbonate-free aqueous solution of tetrabutylammonium acetate was obtained from which the solvent was removed by evaporation. The residual substance was dried under vacuum at a pressure of 10^{-2} mmHg. Remaining traces of water were removed by dissolving the substance in benzene and subsequent evaporation of the solvent. Thus, as is to be seen from the IR spectrum (Figure 2), carbonate- and water-free tetrabutylammonium acetate was obtained.

Acetic acid, p.a., from Merck (pK = 4.76[25]), was used without further purification.

The phenols (see Table III), except of pentachlorophenol, were purified by sublimation. Pentachlorophenol was dried under vacuum (10^{-2} mmHg).

Carbon tetrachloride for spectroscopy was purchased from Merck (Uvasol quality).

IR Spectroscopy. The IR spectra were taken with a grating photospectrometer 325, Bodenseewerk Perkin-Elmer. For the samples a cell with silicon windows was used that is described elsewhere;[28] in the reference beam of the spectrometer, a cell was placed that contained pure solvent. With this cell, a variable layer thickness could be adjusted in order to compensate the solvent bands.

The spectra were digitized by a microcomputer device and transferred to punched tape. This was then used to transfer the data to the CDC Cyber 175 of the Leibniz-Rechenzentrum, Munich, for band evaluation.

Temperature Control of the Cell. A copper pipe was fixed to the sample cell through which a refrigerant was pumped by a thermostat (Haake Type KT33). The actual temperature at the cell was measured by using a PT-100 resistant.

Acknowledgment. We thank the Deutsche Forschungsgemeinschaft and the Fonds der Chemischen Industrie for providing the facilities for this work.

Registry No. 3,5-DCP, 591-35-5; 2,4-DCP, 120-83-2; 2,3-DCP, 576-24-9; 2,3,4-TCP, 15950-66-0; 2,4,5-TCP, 95-95-4; 2,3,5-TCP, 933-78-8; 2,4,6-TCP, 88-06-2; PCP, 87-86-5; *p*-cresol, 106-44-5; acetate, 71-50-1.

(25) Serjeant, E. P.; Dempsey, B. *Ionization Constants of Organic Acids in Aqueous Solutions*; IUPAC Data Series 23; Pergamon: New York, 1978.
(26) Oae, S.; Price, C. D. *J. Am. Chem. Soc.* **1958**, *80*, 4938.
(27) Drahonovsky, J.; Vacek, Z. *Collect. Czech. Chem. Commun.* **1971**, *36*, 3431.
(28) Zundel, G.; Böhner, U.; Fritsch, J.; Merz, H.; Vogt, B. In *Food Analysis*; Gruenwedel, D. W., Whitaker, J. R., Eds.; Marcel Dekker: New York, 1984; Vol. 2, Chapter 10, p 455.

Grand Canonical Monte Carlo Calculations of Thermodynamic Coefficients for a Primitive Model of DNA–Salt Solutions

Pamela Mills, Charles F. Anderson, and M. Thomas Record, Jr.*

Departments of Chemistry and Biochemistry, University of Wisconsin—Madison, Madison, Wisconsin 53706
(Received: April 21, 1986; In Final Form: August 5, 1986)

Monte Carlo (MC) simulations based on the grand canonical ensemble are used to calculate thermodynamic coefficients for a cell model representation of an aqueous solution containing NaDNA and NaCl. The polyion is modeled as an impenetrable cylinder with a uniform, continuous axial charge density, and the small ions are modeled as hard spheres of equal diameter. From a series of MC simulations performed at different salt activities for DNA phosphate concentrations (C_u) over the range 0.005–0.031 mol/dm^3, molar scale mean ionic activity coefficients ($f_\pm^{MC}$) are evaluated for salt concentrations (C_3) over the range 0.002–0.036 mol/dm^3. These results can be accurately represented by an additivity relation: $\ln f_\pm^{MC} = \ln f_\pm^{PB} + \ln f_\pm^{0,MC}$, where $f_\pm^{PB}$ is the mean ionic activity coefficient predicted by the Poisson–Boltzmann (PB) cell model and $\ln f_\pm^{0,MC}$ is a measure of the nonideality due to interactions among the small ions. The theoretical significance of $\ln f_\pm^{0,MC}$ differs from that of the corresponding term in the conventional additivity relation. At each of four fixed salt activities, the dependence of C_3 on C_u predicted by the MC simulations is analyzed to evaluate Γ^{MC}, the preferential interaction coefficient. Values of Γ^{PB} are determined analogously from calculations based on the PB cell model. At each specification of C_3 and C_u, Γ^{MC} is accurately approximated by Γ^{PB}. Consequently, the neglect of small ion correlations by the PB equation does not introduce discrepancies with the thermodynamic predictions of the MC simulations for the model of the polyelectrolyte solution and for the conditions investigated here. The additivity relation for $f_\pm^{MC}$ and $f_\pm^{PB}$ follows directly from the agreement between Γ^{MC} and Γ^{PB}. This finding is another consequence of the status of the preferential interaction coefficient as the fundamental measure of nonideality in a polyelectrolyte solution.

I. Introduction

Monte Carlo (MC) methods can provide detailed information about the microscopic and macroscopic consequences of long-range Coulombic interactions in liquids. Monte Carlo simulations have been used to calculate ion distributions and (in some cases) thermodynamic coefficients for model systems representing electrolyte solutions,[1,2] solutions in contact with a charged plane,[3-7] solutions containing moderately charged spherical micelles,[8,9] and solutions containing rodlike polyions.[10-13] A primary objective of MC studies on polyelectrolyte solutions is to test the accuracy of the small ion distributions predicted by approximate theoretical descriptions, such as the Poisson–Boltzmann (PB) equation. Discrepancies between the MC and PB distributions are generally small for univalent counterions and co-ions. Increasing the size of the small ion assumed in the MC simulations tends to counteract the effect of purely electrostatic correlations on the counterion

(1) Card, D. N.; Valleau, J. P. *J. Chem. Phys.* **1970**, *52*, 6232.
(2) Valleau, J. P.; Cohen, L. K.; Card, D. N. *J. Chem. Phys.* **1980**, *72*, 5942.
(3) Torrie, G. M.; Valleau, J. P. *J. Chem. Phys.* **1980**, *73*, 5807.
(4) Jönsson, B.; Wennerström, H.; Halle, B. *J. Phys. Chem.* **1980**, *84*, 2179.
(5) van Megen, W.; Snook, I. *J. Chem. Phys.* **1980**, *73*, 4656.
(6) Snook, I.; van Megen, W. *J. Chem. Phys.* **1981**, *75*, 4104.
(7) Jönsson, B.; Linse, P.; Åkesson, T.; Wennerström, H. In *Surfactants in Solution*, Mittal, E., Lindman, B., Ed.; Plenum: New York, 1984; p 2023.
(8) Linse, P.; Gunnarsson, G.; Jönsson, B. *J. Phys. Chem.* **1982**, *86*, 413.
(9) Linse, P.; Jönsson, B. *J. Chem. Phys.* **1983**, *78*, 3167.
(10) Bratko, D.; Vlachy, V. *Chem. Phys. Lett.* **1982**, *90*, 434.
(11) LeBret, M.; Zimm, B. H. *Biopolymers* **1984**, *23*, 271.
(12) Murthy, C. S.; Bacquet, R. J.; Rossky, P. J. *J. Phys. Chem.* **1985**, *89*, 701.
(13) Mills, P. A.; Anderson, C. F.; Record, M. T., Jr. *J. Phys. Chem.* **1985**, *89*, 3984.

0022-3654/86/2090-6541$01.50/0